Strong interference effects in the angularly resolved Auger decay and fluorescence emission spectra of the core-excited NO molecule

Ph V Demekhin, I D Petrov, V L Sukhorukov, W Kielich, A Knie, H Schmoranzer, A Ehresmann

Strong interference effects in angularly resolved Auger decay and fluorescence emission spectra of the core-excited NO molecule

Ph V Demekhin[1,2], I D Petrov[2], V L Sukhorukov[2], W Kielich[1], A Knie[1], H Schmoranzer[3], and A Ehresmann[1]

[1] Institute of Physics and CINSaT, University of Kassel, D-34132 Kassel, Germany

[2] Rostov State University of Transport Communications, 344038 Rostov-on-Don, Russia

[3] Department of Physics, Kaiserslautern University of Technology, D-67653 Kaiserslautern, Germany

E-mail: demekhin@physik.uni-kassel.de

Abstract. Angular distributions of the Auger electrons and subsequent fluorescence photons are studied theoretically and experimentally in the vicinity of the core excitations of NO. In the calculations, lifetime vibrational interference and electronic states interference were taken into account *ab initio*. The interference between excitation-deexcitation amplitudes for transitions via symmetry different intermediate resonances $1s^{-1}2\pi^2$ ($^2\Delta$,$^2\Sigma^{\pm}$), which is forbidden in the solid-angle-averaged or magic-angle-recorded decay spectra, plays a crucial role in the formation of the angularly resolved decay spectra. Experimentally, angular distribution parameters for the NO^+ $\left(A\ ^1\Pi \rightarrow X\ ^1\Sigma^+\right)$ fluorescence induced by linearly polarized synchrotron radiation are determined in the vicinity of the N^*O resonance in the Raman regime for core excitation. Theoretical results are in good agreement with the present experimental fluorescence spectra and with available vibrationally and angularly resolved resonant Auger electron spectra.

PACS numbers: 33.80.Eh, 32.80.Hd, 33.50.Dq, 33.80.-b

1. Introduction

A complete photoionization experiment must include the measurement of parameters characterizing the states of both the photoelectron and the residual ion [1]. Alignment and orientation of the residual ion are usually obtained from angular distribution or polarization analysis of fluorescence emitted by a subsequent relaxation of the ion [2, 3, 4]. On the other hand, fluorescence experiments *only* allow a partial wave analysis of the emitted photoelectron waves [5, 6]. Therefore, fluorescence spectroscopy is a very important tool for studying atomic photoionization processes (see, e.g., the review [7]), as a complementary method to photoelectron spectroscopy. Investigation of angularly resolved fluorescence spectra in molecules is an important step in the development of spectroscopy. In our recent works [8, 9] we have investigated polarization of fluorescence (similar to its angular distribution) emitted after core excitation of the closed shell CO molecule. In the present work we report a detailed theoretical and experimental study of angularly resolved fluorescence spectra after core excitation of the open shell NO molecule.

The decay of the core-excited N^*O and NO^* resonances has already been studied by photoelectron spectroscopy (PES) [10, 11, 12, 13], vibrationally resolved constant ionic state spectroscopy (CIS) [14, 15], mass-selective ion-yield (photofragmentation) spectroscopy [16, 17], and photon-induced fluorescence spectroscopy (PIFS) [18, 19]. As has been demonstrated in these studies, lifetime vibrational interference (LVI, [20]) is the dominant effect in the solid-angle-averaged or magic-angle-recorded deexcitation spectra of the resonances. Interference between excitation-deexcitation pathways via different intermediate electronic resonances, known as electronic state interference (ESI, [21]), shows up in the decay spectra only, if the angular averaging is reduced [15, 19]. Excitation of the $1s$ electron to the 2π orbital of NO results in three overlapping doublet states ($^2\Delta$, $^2\Sigma^-$ and $^2\Sigma^+$) accessible by one-photon absorption from the ground state $X\ ^2\Pi$, and decaying into final autoionization states of the 'ion + photoelectron' with different symmetries. Owing to these different symmetries, the ESI between these states

is strictly symmetry-forbidden in the solid-angle-averaged or magic-angle-recorded decay spectra. However, the presence of a new preferential direction in addition to the direction of the polarization vector of the exciting radiation lowers the symmetry of the system (i.e., the molecular axis in the case of oriented molecules or the direction of detection in the case of angularly resolved measurements on randomly oriented molecules). In these cases, the symmetry-different states of the system are not any more orthogonal and they mix, allowing the corresponding amplitudes to interfere [15].

The symmetry-forbidden ESI has been suggested to be responsible for a large disagreement between the $NO^+(X\ ^1\Sigma^+)$ Auger decay spectra of the core-excited N^*O measured in the non-angular averaged regime and computed within the 'standard LVI' theory in [15]. Recently, the symmetry-forbidden ESI in the angularly resolved decay spectra of the core-excited N^*O molecule has been proved [19]. In the present paper we report on a detailed investigation of the ESI in angularly resolved decay spectra of the core-excited NO molecule. As an excellent test of the present theory we, first, reproduce the experimental angular distribution parameters for the $NO^+(X\ ^1\Sigma^+)$ resonant Auger electrons measured in [15]. Angular distribution parameters for the $NO^+(A\ ^1\Pi)$ resonant Auger electrons are also computed. By comparing the presently computed and measured angular distribution parameters for the $NO^+\ (A\ ^1\Pi \rightarrow X\ ^1\Sigma^+)$ fluorescence, we reveal how ESI influences the angularly resolved fluorescence spectra of the core-excited N^*O molecule. Finally, similar effects are also illustrated theoretically for the core-excited NO^* molecule.

2. Theory

The processes relevant to the present study can be schematically represented as the following stepwise cascade decay. Linearly polarized synchrotron radiation with photon energy ω excites the ground state of NO into the N^*O (NO^*) resonances:

$$1s^2 5\sigma^2 2\pi^1\ (X\ ^2\Pi, \Omega_0 v_0 = 0) + \hbar\omega \rightarrow 1s^1 5\sigma^2 2\pi^2\ (^2\Delta/^2\Sigma^{\pm}, \Omega_r v_r), \qquad (1)$$

where Ω is the projection of the total electronic angular momentum along the molecular axis, and v is the vibrational quantum number. The closed shells of NO not participating in the cascade are omitted for brevity. We consider here only two further decays of the intermediate core-excited states: participator Auger decays into the $NO^+(A\ ^1\Pi, \Omega' v')$ and into the $NO^+(X\ ^1\Sigma^+, \Omega'' v'')$ vibronic states:

$$1s^1 5\sigma^2 2\pi^2\ (^2\Delta/^2\Sigma^\pm, \Omega_r v_r) \rightarrow 1s^2 5\sigma^1 2\pi^1\ (A\ ^1\Pi, \Omega' v') + \varepsilon\ell m\mu, \tag{2}$$

$$\hookrightarrow 1s^2 5\sigma^2 2\pi^0\ (X\ ^1\Sigma^+, \Omega'' v'') + \varepsilon\ell m\mu. \tag{3}$$

Here, $\varepsilon\ell m\mu$ are the quantum numbers of the photoelectron, which can be expanded in the asymptotical region via partial waves [22] with fixed projections m and μ of the orbital angular momentum ℓ and spin s, respectively. The resonant population of the $NO^+(A\ ^1\Pi, \Omega' v')$ states (2) takes place via emission of $\varepsilon\pi$ photoelectrons, and that one of the $NO^+(X\ ^1\Sigma^+, \Omega'' v'')$ states (3) via $\varepsilon\sigma/\varepsilon\delta$ photoelectrons. In addition, the direct populations of the $NO^+(A\ ^1\Pi, \Omega' v')$ ionic states in step (2) with emission of $\varepsilon\sigma/\varepsilon\pi$ photoelectrons and of the $NO^+(X\ ^1\Sigma^+, \Omega'' v'')$ ionic states in step (3) with emission of $\varepsilon\sigma/\varepsilon\pi/\varepsilon\delta$ photoelectrons take place via dipole transitions (not indicated for brevity). The $A\ ^1\Pi, \Omega' v'$ states of the NO^+ ion in step (2) decay further via emission of a fluorescence photon hc/λ into the $X\ ^1\Sigma^+, \Omega'' v''$ states:

$$5\sigma^1 2\pi^1\ (A\ ^1\Pi, \Omega' v') \rightarrow 5\sigma^2 2\pi^0\ (X\ ^1\Sigma^+, \Omega'' v'') + hc/\lambda. \tag{4}$$

In order to describe the angular distributions of the photoelectrons and fluorescence photons, we apply the *ab initio* theoretical approach [8].

The angular distribution of photoelectrons after excitation of randomly oriented diatomic molecules by linearly polarized light is given by the well known formula [22]

$$\frac{\mathrm{d}\sigma_{\Omega_1 v_1}(\omega)}{\mathrm{d}\Omega} = \frac{\sigma_{\Omega_1 v_1}(\omega)}{4\pi}\left[1 + \beta^e_{\Omega_1 v_1}(\omega) P_2(\cos\theta)\right], \tag{5}$$

where θ is the angle between the electric field vector of the exciting radiation and the direction of propagation of the outgoing electron emitted into the solid angle $d\Omega$. In Hund's coupling case (a) or (b), the total photoionization cross section, $\sigma_{\Omega_1 v_1}(\omega)$, and

the electron angular distribution parameter, $\beta^e_{\Omega_1 v_1}(\omega)$, entering Eq. (5) can be computed via [8, 22]

$$\sigma_{\Omega_1 v_1}(\omega) = \sum_{\Omega_0 \Omega_1} \sum_{\ell m} \sum_{\mu k} |D_k\left(\Omega_0, \Omega_1 v_1 \varepsilon \ell m \mu\right)|^2, \tag{6}$$

$$\begin{aligned}
\beta^e_{\Omega_1 v_1}(\omega) &= \frac{1}{\sigma_{\Omega_1 v_1}(\omega)} \sum_{\Omega_0 \Omega_1} \sum_{\ell m} \sum_{\ell' m'} \sum_{k k'} \sum_{\mu} (i)^{\ell+\ell'} \\
&\times \sqrt{30(2\ell+1)(2\ell'+1)}(-1)^{\ell'+m+k} e^{-i(\delta_{\ell m} - \delta_{\ell' m'})} \\
&\times \begin{pmatrix} \ell & \ell' & 2 \\ 0 & 0 & 0 \end{pmatrix} \begin{pmatrix} \ell & \ell' & 2 \\ m & -m' & k'-k \end{pmatrix} \begin{pmatrix} 1 & 1 & 2 \\ -k & k' & k-k' \end{pmatrix} \\
&\times D_k\left(\Omega_0, \Omega_1 v_1 \varepsilon \ell m \mu\right) D^*_{k'}\left(\Omega_0, \Omega_1 v_1 \varepsilon \ell' m' \mu\right),
\end{aligned} \tag{7}$$

where $\delta_{\ell m}$ is the phase shift of the electron partial wave.

The amplitude for the population of the $|\Omega_1 v_1\rangle$ ionic state from the initial state $|\Omega_0 v_0\rangle$ in the vicinity of the $|\Omega_r v_r\rangle$ resonances is given by the sum of the direct and all possible resonant amplitudes [8]

$$\begin{aligned}
D_k\left(\Omega_0, \Omega_1 v_1 \varepsilon \ell m \mu\right) = \sqrt{\frac{4\pi^2 \alpha a_0^2 \omega^{\pm 1}}{3 g_{\Omega_0}}} \Bigg\{ & \langle \Omega_1 v_1 \varepsilon \ell m \mu | \mathbf{D}_k | \Omega_0 v_0 \rangle \\
+ \sum_{\Omega_r v_r} & \frac{\langle \Omega_1 v_1 \varepsilon \ell m \mu | \mathbf{H^{ee}} | \Omega_r v_r \rangle \langle \Omega_r v_r | \mathbf{D}_k | \Omega_0 v_0 \rangle}{\omega - E_{\Omega_r v_r} + i \Gamma_{\Omega_r v_r}/2} \Bigg\},
\end{aligned} \tag{8}$$

where $E_{\Omega_r v_r}$ and $\Gamma_{\Omega_r v_r}$ are the energies and natural widths of the vibronic resonances $|\Omega_r v_r\rangle$, respectively; g_{Ω_0} is the statistical weight of the initial electronic state $|\Omega_0\rangle$; $\omega^{\pm 1}$ corresponds to the length and velocity forms of the dipole transition operator $\mathbf{D}$; $\alpha = 1/137.036$ is the fine structure constant; and the square of the Bohr radius $a_0^2 = 28.0028$ Mb converts atomic units for cross sections into megabarn (1 Mb = 10^{-22} m^2). Summation of resonant amplitudes over index v_r accounts for the LVI in the amplitude (8). Although it includes summation over intermediate electronic resonances Ω_r, the ESI is not present in the transition amplitude (8) and, thus, in the total cross section (6), owing to symmetry considerations. Indeed, each of the intermediate electronic resonances $^2\Delta/^2\Sigma^{\pm}(\Omega_r)$ autoionizes into individual continua with

equal symmetry. However, if $\theta \neq 54.7^\circ$ (i.e. not the magic angle), the cross terms with different amplitudes $D_k D^*_{k' \neq k}$, corresponding to the excitation and decay of different electronic resonances, enter the *differential* cross sections (5) via the angular distribution parameter (7), and are responsible for the ESI in the angularly resolved Auger electron spectra.

For randomly oriented diatomic molecules excited by linearly polarized light, the angular distribution of fluorescence emitted via the subsequent $|\Omega_1 v_1\rangle \rightarrow |\Omega_2 v_2\rangle$ transition is given by [8]

$$\frac{\mathrm{d}I^{\Omega_2 v_2}_{\Omega_1 v_1}(\omega)}{\mathrm{d}\Omega} = \frac{I^{\Omega_2 v_2}_{\Omega_1 v_1}(\omega)}{4\pi} \left[1 + \beta 2^{\Omega_2 v_2}_{\Omega_1 v_1}(\omega) P_2(\cos\theta)\right], \tag{9}$$

where θ is the angle between the electric field vector of the exciting radiation and the direction of detection of the fluorescence radiation. Here, the total fluorescence intensity, $I^{\Omega_2 v_2}_{\Omega_1 v_1}(\omega)$, is a product of the total cross section (6) and the fluorescence yield, $\chi^{\Omega_2 v_2}_{\Omega_1 v_1}$ [8]

$$I^{\Omega_2 v_2}_{\Omega_1 v_1}(\omega) = \sigma_{\Omega_1 v_1}(\omega)\, \chi^{\Omega_2 v_2}_{\Omega_1 v_1}, \tag{10}$$

allowing, therefore, no ESI in the solid-angle-averaged fluorescence intensities (10). The equation for the fluorescence angular distribution parameter, $\beta 2^{\Omega_2 v_2}_{\Omega_1 v_1}(\omega)$, reads [8]

$$\begin{aligned}
\beta 2^{\Omega_2 v_2}_{\Omega_1 v_1}(\omega) = {} & \frac{1}{B} \sum_{\Omega_0 \Omega_2} \sum_{q q'} \sum_{\Omega_1 \Omega_1'} \sum_{\ell m \mu} \sum_{k k'} 3(-1)^{k+q'+1} \\
& \times \begin{pmatrix} 1 & 1 & 2 \\ k & -k' & q-q' \end{pmatrix} \begin{pmatrix} 1 & 1 & 2 \\ q & -q' & k-k' \end{pmatrix} \\
& \times \langle \Omega_2 v_2 | \mathbf{D}_{q'} | \Omega_1' v_1 \rangle^* D^*_{k'} \left(\Omega_0, \Omega_1' v_1 \varepsilon \ell m \mu\right) \\
& \times \langle \Omega_2 v_2 | \mathbf{D}_{q} | \Omega_1 v_1 \rangle D_{k} \left(\Omega_0, \Omega_1 v_1 \varepsilon \ell m \mu\right),
\end{aligned} \tag{11}$$

with the normalization coefficient

$$B = \sum_{\Omega_0 \Omega_2} \sum_{\Omega_1 k q} \sum_{\ell m \mu} |\langle \Omega_2 v_2 | \mathbf{D}_q | \Omega_1 v_1 \rangle|^2 |D_k \left(\Omega_0, \Omega_1 v_1 \varepsilon \ell m \mu\right)|^2. \tag{12}$$

Eq. (11) includes the interference (cross terms) between the amplitudes for the population and radiative decay of different degenerate electronic substates of the ion with $\Omega_1 \neq \Omega_1'$ [8].

One should note that in the case of closed shell molecules as, e.g., CO, the cross terms in the fluorescence angular distribution parameter (11) are forbidden [8], similar to the fluorescence angular distribution parameter of the closed shell atoms [6, 7, 23]. For the open shell NO molecule, the cross terms between the $^2\Delta$ and $^2\Sigma^{\pm}$ excitation-deexcitation amplitudes are allowed, and enter the *differential* fluorescence intensities (9) via the angular distribution parameter (11). Thus, ESI can also be observed by measuring the angularly resolved fluorescence spectra of open shell molecules. We emphasize that the absence of the phase difference $(\delta_{\ell m} - \delta_{\ell' m'})$ between partial waves in Eq. (11) as compared to Eq. (7) provides a hint for future partial wave analysis in molecules. The latter fact is the consequence of the integration of the fluorescence intensity over all directions of emission of the photoelectron, since it is not observed in coincidence with the fluorescence photon. For this purpose, determination of the fluorescence angular distribution parameter $\beta 1$ under excitation by circularly polarized radiation is required [5, 6]. We also note, that interference between different partial waves in the $\beta 1$ and $\beta 2$ parameters for the open shell atoms and molecules could make a partial wave analysis more complicated than that for the closed shell ones.

As one can see from Eqs. (7) and (11), the calculation of angular distribution parameters β^e and $\beta 2$ requires the photoionization amplitudes (8) for emission of the partial continuous photoelectron waves with given angular momentum ℓ and its projection m. There are several theoretical approaches enabling to compute these partial waves. In the multichannel Schwinger method (see, e.g., [24, 25] and references therein), continuous channels are the solutions of the Lippmann-Schwinger equation in a basis set of atom-centered Gaussian functions with subsequent one-center partial wave expansion. Another comparatively simple method is known as the one-center approximation (see, e.g., [26, 27] and references therein). It utilizes photoelectron continuous partial waves computed in the field of one atomic center which emits an electron, neglecting thereby interatomic and molecular field effects in the continuum. The latter approximations are absent in the generalization of the atomic random-phase-approximation for diatomic

molecules (see, e.g., [28, 29] and references therein). According to this method, the Hartree-Fock zero order basis set of one-particle wave functions containing both, discrete excited states and continuous partial electron waves, is calculated numerically in prolate spheroidal coordinates in the field of a frozen core ion.

In the present work, partial photoelectron continuous waves were computed by applying the single center (SC) method [8, 9, 30]. In the SC method, a one-particle molecular orbital is represented with respect to a single center of a molecule via expansion in terms of spherical harmonics, and a molecular orbital of a photoelectron in the continuum is a numerical solution of a system of coupled Hartree-Fock equations in spherical coordinates with precise molecular field potentials (see [30] for details). These potentials were calculated using the MO LCAO representation of the occupied shells of a molecule. The resulting photoelectron waves were renormalized in order to satisfy the condition of observable incoming partial waves [31] as described in [8]. Transition amplitudes (8) were computed in the present work within the Franck-Condon approximation. The electronic matrix elements were computed at the equilibrium internuclear distance of the ground state of NO, r_e=2.175 a.u. [32]. In the calculations of the amplitudes (8) relaxation (monopole rearrangement) of the molecular core was taken into account similar to our previous study of the C^*O resonance [8]. The vibrational parts of the amplitudes (8) were computed utilizing *ab initio* potential energy curves from our previous study of NO [18].

3. Experiment

The photon-induced fluorescence spectroscopy (PIFS) has already been applied for polarization analysis of atomic fluorescence [4, 23] and for studying core-excited molecules [8, 18]. The present experimental setup is similar to experiments of [18, 23]. The experiments were performed at the planar elliptical undulator beamline UE56/2-PGM-2 at BESSY II, Berlin. A 400 lines/mm grating was used to monochromatize the synchrotron radiation which was then focused into a differentially pumped target

cell filled with molecular nitric monoxide at room temperature and at a pressure of 33.3 μbar. The exciting-photon energy was varied around the N*O resonance in steps of 25 meV covering the energy range from 398.8 to 401.1 eV. The band width of the exciting radiation was 110 meV FWHM in order to be in the Raman regime of excitation (natural width of the N*O resonances is 124 meV [14]). The exciting-photon energy was calibrated to the known [14, 34] energy positions of the $1s^{-1}2\pi^2(v_r)$ vibrational levels.

Fluorescence radiation between 133 and 157 nm was dispersed by a 1 m normal-incidence monochromator equipped with a 1200 lines/mm grating and recorded by a position-sensitive CsI microchannel-plate detector. The resolution of this 'monochromator-detector' combination was about 0.2 nm. Fluorescence wavelength was calibrated to the known positions of the $A\ ^1\Pi(v') \rightarrow X\ ^1\Sigma^+(v'')$ vibrational bands [35]. The polarization vector $\mathcal{E}$ of the undulator light may be set to horizontal or vertical at this beamline. The fluorescence was observed in the vertical plane perpendicular to the exciting-photon beam. Thus, the spectra recorded with vertical and horizontal polarization correspond to the photon emission parallel ($\parallel$) and perpendicular ($\perp$) to the $\mathcal{E}$ vector, respectively (see the setup geometry in [23]). The detected fluorescence intensity was normalized to the exciting-photon flux yielding at each energy the two spectra $I_\perp(\omega, \lambda)$ and $I_\parallel(\omega, \lambda)$.

In order to analyze energy dependencies of the fluorescence intensities we introduced the integrated fluorescence intensities similar to our previous papers [8, 18]. Relative integrated fluorescence intensities for the $A\ ^1\Pi(v') \rightarrow X\ ^1\Sigma^+(v'')$ bands at a given exciting-photon energy, $I_\parallel(\omega)$ and $I_\perp(\omega)$, have been determined by integrating the measured fluorescence intensities, $I_\parallel(\omega, \lambda)$ and $I_\perp(\omega, \lambda)$, over the wavelength intervals centered around the vibrational band positions

$$I_{\parallel/\perp}(\omega) = \int I_{\parallel/\perp}(\omega, \lambda)\ \mathrm{d}\lambda. \tag{13}$$

The angular distribution parameter $\beta 2(\omega)$ and the total fluorescence intensity $I(\omega)$ for the present experimental geometry can be obtained from Eq. (9) by setting $\theta = 0^\circ$ and

90°, and are given by

$$I(\omega) = \frac{I_{\parallel}(\omega) + 2I_{\perp}(\omega)}{3}, \tag{14}$$

$$\beta 2(\omega) = 2\frac{I_{\parallel}(\omega) - I_{\perp}(\omega)}{I_{\parallel}(\omega) + 2I_{\perp}(\omega)}. \tag{15}$$

The present experimental results are discussed in subsection 4.2.

4. Results and discussion

Resonant photoabsorption and different resonant photoelectron spectra of N^*O are discussed in details in, e.g., [13, 14, 15, 36]. For clearness of the present discussion, an overview of the N^*O resonant photoionization spectrum from [18] is depicted in panel (a) of Fig. 1. In what follows we analyze the impact of ESI on angularly resolved decay spectra of the core-excited NO molecule. The $NO^+(X\ ^1\Sigma^+)$ resonant Auger electron spectra of N^*O are discussed in subsection 4.1, and the $NO^+(A\ ^1\Pi)$ Auger decay and $A\ ^1\Pi \rightarrow X\ ^1\Sigma^+$ fluorescence emission spectra of N^*O – in subsection 4.2. The $NO^+(A\ ^1\Pi)$ Auger decay and $A\ ^1\Pi \rightarrow X\ ^1\Sigma^+$ fluorescence emission spectra of the $O(1s \rightarrow 2\pi)$ core-excitation of NO^* are investigated theoretically in subsection 4.3. In order to illustrate the influence of ESI on the computed decay spectra and to reveal different contributions, the present calculations were performed in different approximations:

(i) *Direct*: only direct photoionization channels were accounted for;

(ii) *Separate(Res)*: only resonant photoionization channels were accounted for separately for each intermediate electronic resonance. In this case, computed angular distribution parameters become independent of the exciting-photon energy even though the nuclear vibrational motion and LVI are included [8, 9];

(iii) *NoESI(Dir+Res)*: the direct and all electronic resonant amplitudes were incorporated incoherently, by weighting the angular distribution parameters computed in the '*Direct*' and '*Separate(Res)*' approximations by the corresponding cross sections;

(iv) *ESI(Res)*: interference between all resonant electronic amplitudes was taken into account;

(v) *ESI(Dir+Res)*: interference between the direct and all resonant amplitudes was taken into account.

4.1. Angularly resolved $X\ ^1\Sigma^+$ Auger spectra of N^*O

The accuracy of the present theoretical approach was checked by computing the participator Auger spectra of the N^*O resonance into the $NO^+(X\ ^1\Sigma^+, v'')$ states. The presently computed angular-averaged Auger decay spectra are in good agreement with the magic-angle recorded Auger intensities of [13, 15] (not shown here for brevity). The presently computed angular distribution parameters $\beta^e_{Xv''}$ for Auger electrons are compared with the experimental [15] ones in Fig. 1. Panel (b) of the figure depicts the experimental $\beta^e_{Xv''}$ values as functions of the vibrational quantum number v'', measured in [15] at different exciting-photon energies. These energies are indicated in the resonant photoionization cross section in panel (a) by the vertical arrows. Panel (c) of Fig. 1 shows the $\beta^e_{Xv''}$ parameters computed in the most accurate approximation '*ESI(Dir+Res)*'. Fig. 1 illustrates good agreement between the present theory and experiment [15]. This enables us to clarify the reasons responsible for the disagreement between the $\beta^e_{Xv''}$ parameters computed and measured in [15] (see figure 12 and relevant discussion in [15]).

Parameters $\beta^e_{Xv''}(\omega)$ computed in different approximations for the vibronic states $X\ ^1\Sigma^+, v'' = 0$ and 1 are depicted in Fig. 2 as functions of the exciting-photon energy. Namely for these two states the 'standard LVI' theory of [15] fails to predict the exciting-photon energy dependencies observed in the experiments. The $\beta^e_{Xv''}$ values computed separately for the $^2\Delta$ and $^2\Sigma^+$ resonances are +0.276 and –0.133, respectively (shown in Fig. 2 by horizontal bars). Due to the 'filtering effect' [14] in core excitation spectra of NO based on selection rules in the Auger decay matrix element, the $^2\Sigma^-$ resonance is not 'visible' in the $X\ ^1\Sigma^+$ final Auger state. Interference between the $^2\Delta$ and $^2\Sigma^+$

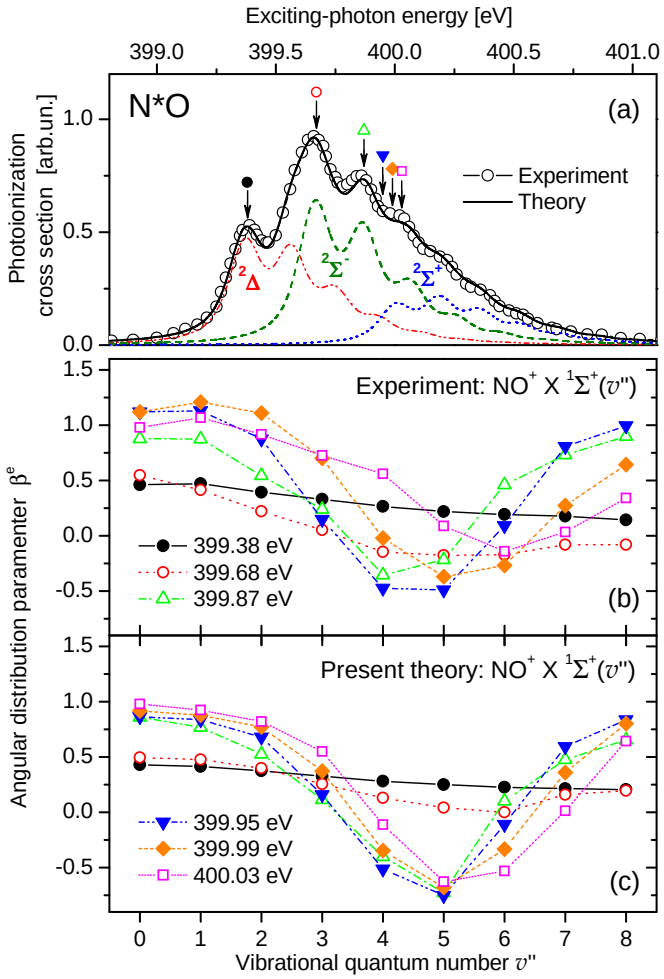

Figure 1. (Color online) Panel (a): experimental and theoretical photoionization cross sections for the N*O resonance (data from [18]). The individual contributions from the transitions via the $^2\Delta$ (dash-dot-dot), $^2\Sigma^-$ (dash), and $^2\Sigma^+$ (dot) states are also shown. The exciting-photon energies selected in [15] for measurements (panel (b)) are indicated by vertical arrows. Panels (b) and (c): angular distribution parameters for the $NO^+X\ ^1\Sigma^+(v'')$ photoelectrons measured in [15] and computed in the present work as functions of the vibrational quantum number v'' for selected exciting-photon energies (indicated in panel (a)) in the vicinity of the N*O resonance.

electronic resonances causes the counterintuitive exciting-photon energy dependencies of the computed $\beta^e_{Xv''}(\omega)$ parameters ('*ESI(Res)*' approximation in Fig. 2). Indeed, one would expect that the computed parameters must decrease with energy in between these two resonances, following their individual $\beta^e_{Xv''}$ values (horizontal bars). The computed parameters, however, increase first with the energy, exhibiting already trends observed

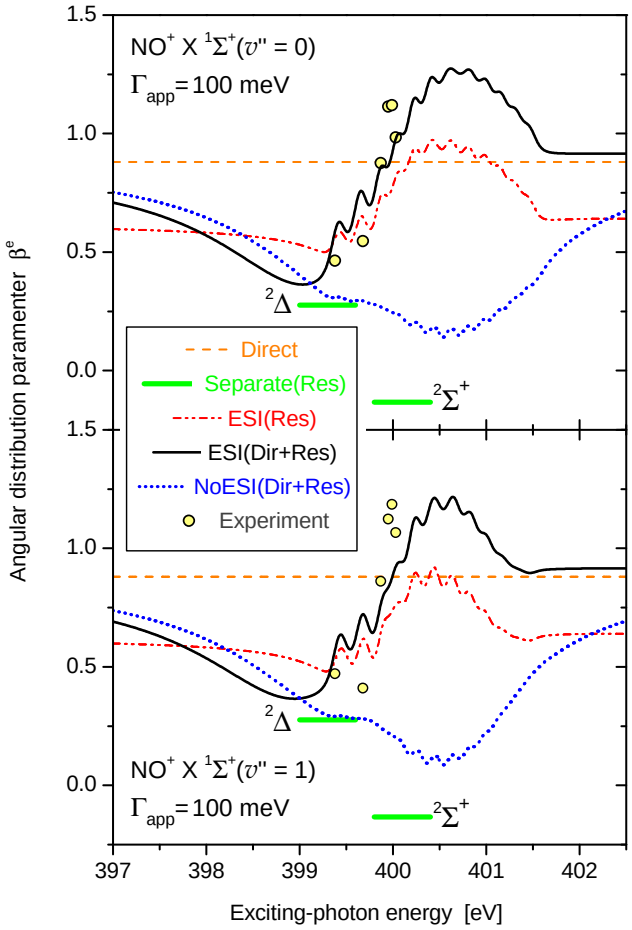

Figure 2. (Color online) Angular distribution parameters for the $NO^+ X\ ^1\Sigma^+(v'' = 0$ and 1) photoelectrons measured in [15] and computed in different approximations in the vicinity of the N^*O resonance. Computed parameters were convolved with a Gaussian of 100 meV FWHM.

in the experiment [15] (shown by open circles).

The cross terms between $^2\Delta$ and $^2\Sigma^+$ resonant amplitudes in Eq. (7) are responsible for this effect. Due to the energy denominator, the resonant amplitude in Eq. (8) changes its sign across the resonance. At exciting-photon energies below the $^2\Delta$ resonance, both amplitudes have the same sign. At energies above the $^2\Sigma^+$ resonance, they again have the same sign (but opposite to the previous one). Thus, in these energy ranges, the cross terms are positive. In between the $^2\Delta$ and $^2\Sigma^+$ resonances, the amplitudes have opposite signs, and the cross terms are negative. The change in sign of the cross terms in Eq. (7) across the N^*O resonance from positive to negative and again to positive

is responsible for the change of the ESI from constructive to destructive and again to constructive.

The individual contributions of direct photoionization to the angular distribution parameters are illustrated in Fig. 2 by dashed curves. Being included in the calculations in addition to the two electronic resonant channels ('*ESI(Dir+Res)*' approximation), direct photoionization brings the computed $\beta^e_{Xv''}(\omega)$ parameters into good agreement with experiment [15]. The large impact of the weak direct photoionization in the case of $v'' = 0$ and 1 final vibronic states is caused by the following reasons. The Auger electron intensities of the N*O resonance are spread over a wide range of final vibrational states $X\ ^1\Sigma^+, v''$ (up to $v'' = 13$ [13, 15]). In addition, the $v'' = 0$ and 1 states have relatively low resonant population. As a result, the direct photoionization of these states is not negligibly small in comparison with the resonant ones. In order to illustrate the complete effect of the ESI, the $\beta^e_{Xv''}(\omega)$ parameters computed within the '*NoESI(Dir+Res)*' approximation are also depicted in Fig. 2 by dotted curves (to be compared with the solid curves). The dotted curves somehow follow the individual $\beta^e_{Xv''}$ values of both $^2\Delta$ and $^2\Sigma^+$ resonances and resemble the 'standard LVI' theory of [15] (note, that the '*NoESI(Dir+Res)*' approximation includes also an incoherent contribution from the direct photoionization, which is absent in the 'standard LVI' theory of [15]).

*4.2. Angularly resolved $A\ ^1\Pi$ Auger and $A\ ^1\Pi \rightarrow X\ ^1\Sigma^+$ fluorescence spectra of N*O*

In the present experiment, the following two vibrational band progressions of the $A\ ^1\Pi(v') \rightarrow X\ ^1\Sigma^+(v'')$ fluorescence have been resolved in the fluorescence range between 133 and 157 nm: $v' = 0 \rightarrow v'' = 0 \ldots 4$ and $v' = 1 \rightarrow v'' = 0 \ldots 2$ (see overview of the fluorescence spectrum, e.g., in [35]). The weak progression $v' = 2 \rightarrow v'' = 1, 2$ was also resolved with very low signal-to-noise ratio (not discussed later). From Eq. (10) it is obvious that the exciting-photon energy dependence of the total fluorescence intensity is determined only by the cross section for population of the initial fluorescence state,

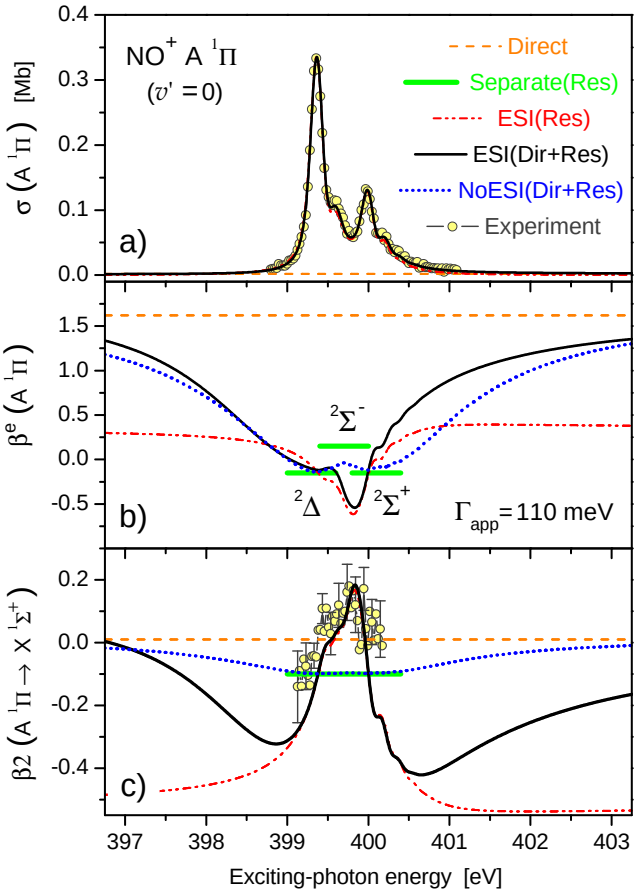

Figure 3. (Color online) Results of the present calculations performed in different approximations (see text) together with the present experimental results. Computed parameters were convolved with a Gaussian of 110 meV FWHM. Panel (a): cross section for the population of the NO^+ $A\ ^1\Pi(v'=0)$ vibronic state across the N^*O resonance. Experimental data are normalized to the theory at the maximum. Panel (b): angular distribution parameter for the NO^+ $A\ ^1\Pi(v'=0)$ photoelectrons. Panel (c): angular distribution parameter for the $A\ ^1\Pi(v'=0) \rightarrow X\ ^1\Sigma^+(v'')$ fluorescence bands progression. No normalization is required for experimental $\beta 2$ values.

and is independent of the final fluorescence state. Similarly, the fluorescence angular distribution parameters (11) are independent of the vibrational quantum number of the final fluorescence state [8, 9]. As a consequence, similar exciting-photon energy dependencies of the fluorescence intensities $I_{Av'}^{Xv''}(\omega)$ and angular distribution parameters $\beta 2_{Av'}^{Xv''}(\omega)$ have been observed for each vibrational band within a given $A\ ^1\Pi(v' = const) \rightarrow X\ ^1\Sigma^+(v'')$ progression. Therefore, we discuss hereafter the fluorescence

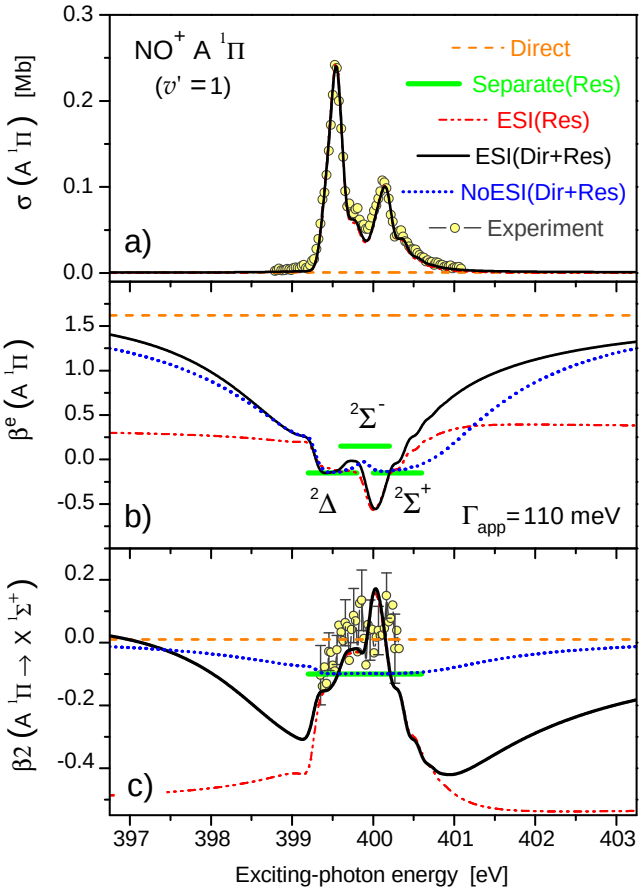

Figure 4. (Color online) Parameters computed and measured for the NO^+ $A\ ^1\Pi$ ($v' = 1$) state across the N^*O resonance (see notations in Fig. 3).

bands 0–2 ($\lambda \approx 146.2$ nm) and 1–2 ($\lambda \approx 143.0$ nm) only, which represent both presently resolved progressions.

Cross sections $\sigma_{Av'}(\omega)$ and angular distribution parameters for the photoelectrons $\beta^e_{Av'}(\omega)$ and for the fluorescence $\beta 2^{Xv''}_{Av'}(\omega)$ computed within the most accurate approximation '*ESI(Dir+Res)*' for the final states NO^+ $A\ ^1\Pi(v' = 0$ and 1) are depicted in Figs. 3 and 4, respectively, by solid lines. The two maxima in the computed cross sections $\sigma_{Av'}(\omega)$ at lower and higher exciting-photon energies correspond to the decay of the $^2\Delta$ and $^2\Sigma^+$ resonances, respectively [18]. Weak contributions from the $^2\Sigma^-$ resonance are located between the two maxima but blended. This is due to the cancellation of the direct and exchange Coulomb integrals in the corresponding Auger decay matrix element [18]. The relative electronic probabilities for the excitation and

decay of the $^2\Sigma^+$, $^2\Delta$, and $^2\Sigma^-$ states computed in the present work are equal to $1:2:0.1$, respectively. One can see that the weak direct photoionization influences the computed $\sigma_{Av'}(\omega)$ negligibly (solid and dash-dot-dotted curves in panels (a) are practically indistinguishable). The same holds for the computed parameters $\beta^e_{Av'}(\omega)$ and $\beta 2^{Xv''}_{Av'}(\omega)$ close to the resonance. The weak direct photoionization influences the angular distribution parameters noticeably only for large energy detunings from the resonance (cf solid and dash-dot-dotted curves in panels (b) and (c)). Due to an almost diagonal Franck-Condon matrix for Auger decay $| < v'|v_r > |^2$ (corresponding potential energy curves are very similar around the respective equilibrium internuclear distances), the resonant amplitude is gathered in a few final vibrational states with $v' \approx v_r$ [18]. As a result, the resonant population amplitudes in this case are much larger than the direct ones (contrary to the $X\ ^1\Sigma^+$ final Auger state considered in subsection 4.1).

Angular distribution parameters computed for the direct (*Direct*) and for each electronic resonant photoionization channel separately (*Separate(Res)*) are depicted in Figs. 3 and 4 by dashed lines and horizontal bars, respectively (note, that the $\beta 2^{Xv''}_{Av'}$ values for the fluorescence angular distribution parameter are equal to -0.1 for all electronic resonances). These angular distribution parameters were weighted by the corresponding cross sections and are depicted in panels (b) and (c) by dotted curves ('*NoESI(Dir+Res)*' approximation). As expected, neglecting the ESI does not change the computed cross sections (not shown in the figures). One can see that neglecting the ESI changes the computed $\beta^e_{Av'}(\omega)$ and $\beta 2^{Xv''}_{Av'}(\omega)$ dispersions drastically. The ESI is responsible for the curvature changes of the dispersions between the $^2\Delta$ and $^2\Sigma^+$ resonances from concave to convex and vice versa. Moreover, for the $\beta 2^{Xv''}_{Av'}(\omega)$ parameter, ESI also changes its sign twice across the resonance. As discussed above, in the case of the $\beta 2^{Xv''}_{Av'}(\omega)$ parameter, ESI is described by the cross terms in Eq. (11) and is allowed between the $^2\Delta$ and $^2\Sigma^\pm$ amplitudes. These amplitudes change their signs across the resonances, causing the illustrated effect.

The total fluorescence intensities $I^{Xv''}_{Av'}(\omega)$ and angular distribution parameters

$\beta 2^{Xv''}_{Av'}(\omega)$ measured for the 0–2 and 1–2 fluorescence bands are depicted in Figs. 3 and 4, respectively, by open circles. From panels (a) it is evident that the measured fluorescence intensities are in very good agreement with the computed cross sections for the population of the initial fluorescence states. The measured $\beta 2^{Xv''}_{Av'}(\omega)$ parameters are shown in panels (c) only at those energies where the present count rate (signal-to-noise ratio) was reliable (error bars $\Delta\beta 2$ within ± 0.1). One can see that the measured absolute values and dispersions of the $\beta 2^{Xv_2}_{Av_1}(\omega)$ parameters are also in good agreement with those computed by including ESI between three intermediate resonances (solid curves). Although the experimental error bars are still large, the present measurement supports the effect of ESI illustrated by the theory, including the changes of its sign (the present experimental uncertainties are less than the difference between the $\beta 2^{Xv''}_{Av'}(\omega)$ parameters computed in the *NoESI(Dir+Res)* and *ESI(Dir+Res)* approximations).

*4.3. Angularly resolved $A\ ^1\Pi$ Auger and $A\ ^1\Pi \rightarrow X\ ^1\Sigma^+$ fluorescence spectra of NO**

The relative electronic probabilities for the excitation and decay of the $^2\Sigma^+$, $^2\Delta$, and $^2\Sigma^-$ states of NO* computed in the present work are equal to $1:2:0.03$, respectively. These resonances appear in the spectra in the following energetical order: $^2\Sigma^-$, $^2\Delta$, and $^2\Sigma^+$ [37, 38] (contrary to their order in the N*O resonance). Due to the small excitation-deexcitation rate for the $^2\Sigma^-$ resonance, only the $^2\Delta$ and $^2\Sigma^+$ resonances are again responsible here for the main interference effects. The resonant $O(1s \rightarrow 2\pi)$ excitation amplitude is spread over a wide range of intermediate vibrational states, up to $v_r \approx 20$. In addition, potential energy curves for the intermediate and final states are considerably shifted in R relatively to each other [18], resulting in small Franck-Condon factors for Auger decay $| < v'|v_r > |^2$. Therefore, it is expected that the influence of the weak direct photoionization can be observed even in the total (magic angle) cross sections, similarly to the $O(1s \rightarrow 2\pi)$ excitation of CO* [9, 39].

Present theoretical results for the NO* resonance are summarized in Figs. 5 and 6 for the final states $NO^+\ A\ ^1\Pi(v_1 = 0$ and 1) with the highest population probabilities. The

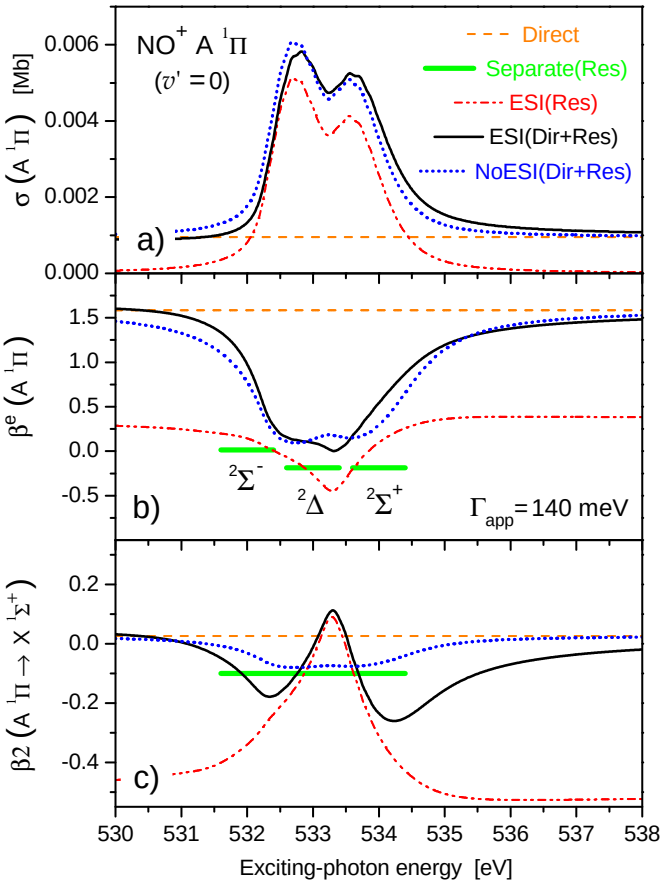

Figure 5. (Color online) Parameters computed for the NO^+ $A\ ^1\Pi$ ($v' = 0$) state across the NO^* resonance (see notations in Fig. 3).

computed parameters are convolved with a Gaussian of 140 meV FWHM, corresponding to the experimental resolution expected at these energies [18]. From panels (a) of these figures it is evident that the direct photoionization is not negligibly small in the case of the $O(1s \rightarrow 2\pi)$ core-excitation of NO^* (cf dashed lines and dash-dot-dotted curves). Being included coherently with the resonant photoionization, it causes destructive and constructive interferences at the low and high energy sides of the resonance, respectively (cf dotted and solid curves in panels (a) of Figs. 5 and 6). As mentioned above, the interference between intermediate electronic resonances is forbidden by symmetry in the total cross sections (the dotted curves in panels (a) are simply shifted by the constant direct photoionization relatively to the dash-dot-dotted curves).

The symmetry-forbidden ESI between the $^2\Delta$ and $^2\Sigma^+$ resonant amplitudes is

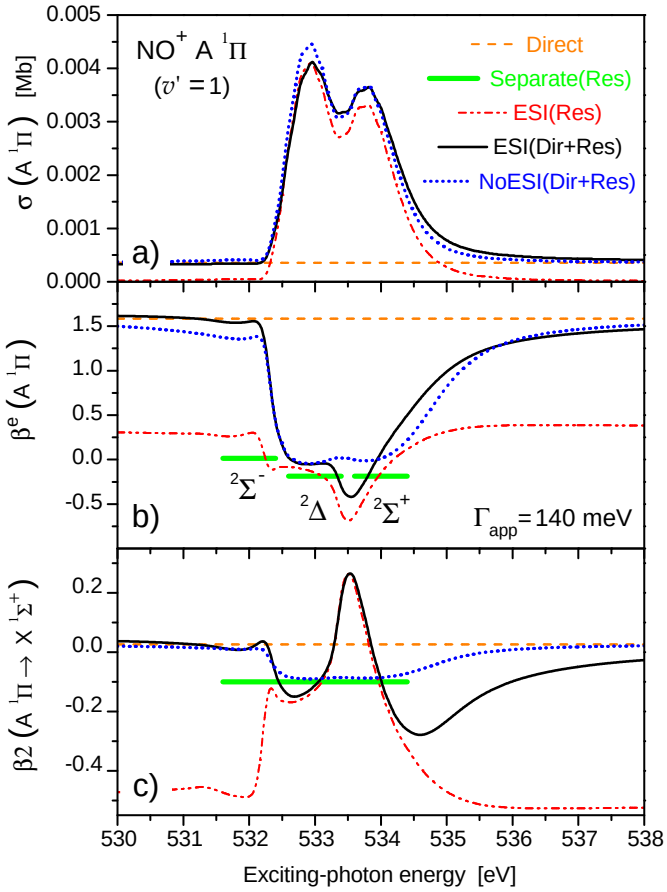

Figure 6. (Color online) Parameters computed for the NO^+ $A\ ^1\Pi$ ($v' = 1$) state across the NO^* resonance (see notations in Fig. 3).

clearly visible in the angular distribution parameters $\beta^e_{Av'}(\omega)$ and $\beta 2^{Xv''}_{Av'}(\omega)$ depicted in panels (b) and (c) of Figs. 5 and 6. Similarly to the case of the N^*O excitation, it changes drastically the exciting-photon energy dependencies of the angular distribution parameters (cf dotted and solid curves). Considerable influence of the direct photoionization on the angular distribution parameters in the on- and off-resonance excitation regimes is also evident from these figures (cf dash-dot-dotted and solid curves). Finally, clear fingerprints of the very weak $^2\Sigma^-$ resonance can be seen for the $v' = 1$ final state (Fig. 6), as the asymmetric resonant feature in the angular distribution parameters at exciting-photon energy of around 532.25 eV.

5. Conclusions

Dispersions of the angular distribution parameters for the NO^+ $X\ ^1\Sigma^+$ and $A\ ^1\Pi$ photoelectrons and for the $A\ ^1\Pi \rightarrow X\ ^1\Sigma^+$ fluorescence have been calculated in the vicinity of the N^*O (NO^*) resonances *ab initio*. The angular distribution parameters of the resonantly excited $NO^+(A\ ^1\Pi \rightarrow X\ ^1\Sigma^+)$ fluorescence have been determined in the vicinity of the N^*O resonance in the Raman regime for core excitation by means of photon-induced fluorescence spectroscopy (PIFS). The present calculations are in good agreement with the presently measured angularly resolved fluorescence spectra and enable us to interpret vibrationally and angularly resolved Auger decay spectra of [15].

It is illustrated by the theory that the interference between the amplitudes for excitation and decay of neighboring core-excited N^*O and NO^* resonances of different symmetries plays a significant role in the formation and interpretation of their angularly resolved Auger electron and fluorescence emission spectra, although it is symmetry-forbidden in the solid-angle-averaged spectra. The interference between the weak direct and dominant resonant photoionization channels is also very important, influencing the non-angle-averaged spectra not only in the off-resonance detuning regime, but in proximity of the resonances, too. These interferences determine both, the absolute values of the parameters for angular distributions of photoelectrons and fluorescence photons and their exciting-photon energy dependencies across the resonances.

Acknowledgments

This work was performed within the European Community's 7^{th} Framework Programme (Marie Curie project no PIIF-GA-2008-219224), by the Deutsche Forschungsgemeinschaft (DFG) project (EH 187/16-1), and by the Bundesministerium für Bildung und Forschung (BMBF) project (05KS7RK1). The Helmholtz-Zentrum Berlin is gratefully acknowledged for travel expense support by Bundesministerium für

Bildung und Forschung (BMBF) (contract no 05 ES3XBA/5). VLS and IDP would like to thank the Institute of Physics, University of Kassel for the hospitality during their stay there.

References

[1] Cherepkov N A and Semenov S K 2004 *J. Phys. B: At. Mol. Opt. Phys.* **37** 1267–72

[2] Berezhko E G and Kabachnik N M 1977 *J. Phys. B: At. Mol. Phys.* **10** 2467–77

[3] Lagutin B M, Petrov I D, Sukhorukov V L, Kammer S, Mickat S, Schill S, Schartner K-H, Ehresmann A, Shutov Y A, Schmoranzer H 2003 *Phys. Rev. Lett.* **90** 073001

[4] Lagutin B M, Petrov I D, Sukhorukov V L, Demekhin Ph V, Zimmermann B, Mickat S, Kammer S, Schartner K-H, Ehresmann A, Shutov Y A, Schmoranzer H 2003 *J. Phys. B: At. Mol. Opt. Phys.* **36** 3251–68

[5] Schill R, Hasselkamp D, Kammer S, Mickat S, Zimmermann B, Schartner K-H, Ehresmann A, Shutov Y A, Schmoranzer H, Schlüter M, Shutov Y A, Lagutin B M, Sukhorukov V L 2003 *J. Phys. B: At. Mol. Opt. Phys.* **36** L57–61

[6] Schartner K-H, Schill R, Hasselkamp D, Mickat S, Kammer S, Werner L, Klumpp S, Ehresmann A, Schmoranzer H, Lagutin B M, Sukhorukov V L 2005 *J. Phys. B: At. Mol. Opt. Phys.* **38** 4155–70

[7] Kabachnik N M, Fritzsche S, Grum-Grzhimailo A N, Meyer M, Ueda K 2007 *Phys. Rep.* **451** 155–233

[8] Demekhin Ph V, Petrov I D, Sukhorukov V L, Kielich W, Reiss P, Hentges R, Haar I, Schmoranzer H and Ehresmann A 2009 *Phys. Rev. A* **80** 063425; Erratum: 2010 *Phys. Rev. A* **81** 069902(E).

[9] Demekhin Ph V, Petrov I D, Tanaka T, Hoshino M,Tanaka H, Ueda K, Kielich W, Ehresmann A 2010 *J. Phys. B: At. Mol. Opt. Phys.* **43** 065102

[10] Carroll T X, Anderson S E, Ungier L, Thomas TD 1987 *Phys. Rev. Lett.* **58** 867–70

[11] Carroll T X and Thomas T D 1992 *J. Chem. Phys.* **97** 894–9

[12] Carroll T X, Coville M, Morin P, Thomas T D 1994 *J. Chem. Phys.* **101** 998–1005

[13] Kukk E, Snell G, Bozek J D, Cheng W T, Berrah N 2001 *Phys. Rev. A* **63** 062702

[14] Wang H, Fink R F, Piancastelli M N, Hjelte I, Wiesner K, Bässler M, Feifel R, Björneholm O, Miron C, Giertz A, Burmeister F, Sorensen S L, Svensson S 2001 *J. Phys. B: At. Mol. Opt. Phys.* **34** 4417–26

[15] Wang H, Fink R F, Piancastelli M N, Bässler M, Hjelte I, Björneholm O, Burmeister F, Feifel R, Giertz A, Miron C, Sorensen S L, Wiesner K, Svensson S 2003 *Chem. Phys.* **289** 31–44

[16] Erman P, Hatherly P A, Karawajczyk A, Köbley U, Rachlew-Källney E, Stankiewicz M, Franzén K Y, 1996 *J. Phys. B: At. Mol. Opt. Phys.* **29** 1501–13

[17] Yu SW, Stolte W C, Guillemin R, Öhrwall G, Tran I C, Piancastelli M N, Feng G, Lindle D W 2004 *J. Phys. B: At. Mol. Opt. Phys.* **37** 3583–92

[18] Ehresmann A, Kielich W, Werner L, Demekhin Ph V, Omel'yanenko D V, Sukhorukov V L, Schartner K-H, Schmoranzer H 2007 *Eur. Phys. J. D* **45** 235–46

[19] Demekhin Ph V, Petrov I D, Sukhorukov V L, Kielich W, Knie A, Schmoranzer H, Ehresmann A 2010 *Phys. Rev. Lett.* **104** 243001.

[20] Gel'Mukhanov F K, Mazalov L N, Kondratenko A V 1977 *Chem. Phys. Lett.* **46** 133–7

[21] Cesar A and Ågren H 1992 *Phys. Rev. A* **45** 2833–41

[22] Cherepkov N A 1981 *J. Phys. B: At. Mol. Phys.* **14** 2165–77

[23] Schmoranzer H, Lauer S, Vollweiler F, Ehresmann A, Sukhorukov V L, Lagutin B M, Petrov I D, Demekhin Ph V, Schartner K-H, Magel B, Mentzel G 1997 *J. Phys. B: At. Mol. Opt. Phys.* **30** 4463–80

[24] Bonhoff K, Bonhoff S, Schimmelpfennig B, Nestmann B, Blum K 1998 *J. Phys. B: At. Mol. Opt. Phys.* **31** 1511–22.

[25] Bonhoff S, Bonhoff K, Blum K 1999 *J. Phys. B: At. Mol. Opt. Phys.* **32** 1139–49

[26] Rolles D, Prümper G, Fukuzawa H, Liu X-J, Pešič Z D, Fink R F, Grum-Grzhimailo A N, Dumitriu I, Berrah N, Ueda K 2008 *Phys. Rev. Lett.* **101** 263002

[27] Fink R F, Piancastelli M N, Grum-Grzhimailo A N, Ueda K 2009 *J. Chem. Phys.* **130** 014306

[28] Semenov S K and Cherepkov N A 2003 *J. Phys. B: At. Mol. Opt. Phys.* **36** 1409–22

[29] Semenov S K, Kuznetsov V V, Cherepkov N A, Bolognesi P, Feyer V, Lahmam-Bennani A, Staicu Casagrande M E, Avaldi L 2007 *Phys. Rev. A* **75** 032707

[30] Demekhin Ph V, Omel'yanenko D V, Lagutin B M, Sukhorukov V L, Werner L, Ehresmann A, Schartner K-H, Schmoranzer H 2007 *Optics and Spectroscopy* **102** 318–29

[31] Starace A F 1982 *Theory of atomic photoionization*, *Handbuch der Physik* Vol. 31 (Berlin: Springer)

[32] Huber K P and Herzberg G 1979 *Molecular Spectra and Molecular Structure. IV. Constants of Diatomic Molecules* (New York: Van Nostrand-Reinhold)

[33] Ehresmann A, Werner L, Klumpp S, Lucht S, Schmoranzer H, Mickat S, Schill R, Schartner K-H, Demekhin Ph V, Lemeshko M P, Sukhorukov V L 2006 *J. Phys. B: At. Mol. Opt. Phys.* **39** 283–304

[34] Püttner R, Dominguez I, Morgan T J, Cisneros C, Fink R F, Rotenberg E, Warwick T, Domke M, Kaindl G, Schlachter A S 1999 *Phys. Rev.* A **59** 3415–23

[35] Maier II W B and Holland R F 1971 *J. Chem. Phys.* **54** 2693–714

[36] R. Fink 1997 *J. Chem. Phys.* **106** 4038–52

[37] Wight G R and Brion C E 1974 *J. Electr. Spectr. Relat. Phenom.* **4** 313–25

[38] Kosugi N, Adachi J, Shigemasa E, Yagishita A 1992 *J. Chem. Phys.* **97** 8842–9

[39] Feifel R, Tanaka T, Hoshino M, Tanaka H, Tamenori Y, Carravetta V, Ueda K 2006 *Phys. Rev. A* **74** 062717